Rock physics guided velocity model building: A 2D field data example

Huy Le, Anshuman Pradhan, Nader C. Dutta, Biondo Biondi, Tapan Mukerji, and Stewart A. Levin

ABSTRACT

In our previous report we developed a rock physics workflow that combines various sources of data such as well logs, mud weights, Bottom Hole Temperature, and basin history to model pore pressure-velocity relationship, taking into account both shale diagenesis and mechanical compaction. In this report, we apply this workflow to a field data collected from the Gulf of Mexico and build velocity models for imaging and inversion. We examine a number of different pore pressure gradient scenarios and velocity models. We access the feasibility of these models based on the quality of their resulting images and flatness of angle gathers. Our results show that rock physics and basin modeling integration gives a velocity model that not only fits the observed data better but also is geologically more plausible.

INTRODUCTION

Anisotropic imaging has been shown to be necessary in many successful exploration applications, particularly in the Gulf of Mexico, where alignment of clay minerals in shales and the effect of layering both imply transverse isotropy. Additionally, salt bodies can cause stress perturbations that further complicate velocity variation.

Building anisotropic velocity models for imaging is a challenge due to uncertainties in anisotropic parameters. Conventional velocity analysis and tomography of surface seismic might not provide a satisfactory answer because a number of models could equally well explain the observed data. Such is also the case with full waveform inversion (FWI). All of these inversion schemes rely heavily on the assumption that the initial model is close to the true model. When this assumption does not apply, there is a high possibility of obtaining a velocity model that satisfies the imposed convergence criterion but may be geologically and physically improbable. The rock physics guided workflow we use imposes additional constraints on velocities that not only satisfy the gather flattening criterion but also require the model to be geologically and physically possible.

Anisotropic velocity models can be built with forward modeling using rock physics principles, geomechanics, and basin modeling. Bachrach (2010) used differential effective medium (DEM) theory from rock physics combined with well logs and empirical

models of shale diagenesis to build anisotropic velocity models. Petmecky et al. (2009) derived anisotropic velocities for imaging from a 3D basin modeler to capture the pressure, depositional, fluid flow, and salt movement histories of a basin. Matava et al. (2016) used finite elastic deformation theory to calculate the effect of stress anomalies caused by salt movements on velocity.

Recent developments in anisotropic velocity model building show that integrating additional data, such as rock physics and pore pressures, can constrain the velocity inversion process. Dutta et al. (2015) combined rock physics and pore pressure-velocity models to create velocity bounds for tomography. These constraints not only reduce uncertainty in the tomography process, but also produce a velocity model that is able to predict physical pore pressure. For a review on geopressure prediction, refer to Dutta (2002). This is an extra constraint that forces the vertical velocity to be within a physically expected range such as yielding a pore pressure that is bounded below by hydrostatic pore pressure and above by fracture pressure. In addition, the use of rock physics compliant velocity model enables us to estimate vertical velocity without having to rely on normal moveout analysis, which often produce poor estimates of velocity. Li et al. (2016) used stochastic rock physics modeling (Bachrach, 2010) to build model covariance matrices to constrain wave equation migration velocity analysis (WEMVA). Following Dutta et al. (2015), we have developed a workflow that combines rock physics, basin modeling, and pore pressure constraints to improve velocity models for imaging (Le et al., 2017a). In this report, we apply this workflow to a 2D field data acquired from the Gulf of Mexico.

ROCK PHYSICS WORKFLOW

In this section we briefly describe our rock physics workflow. The workflow applies to the diagenesis of shale, particularly, the transformation of smectite into illite as a result of burial diagenesis. The rock model consists of, therefore, a matrix solid (smectite and illite), and a pore fluid (water). Two processes can affect pore pressure. First, as sediments deposit, mechanical compaction causes porosity to reduce. Second, when clayey rocks are buried to deeper depths and temperature reaches activation threshold, the transformation from smectite to illite happens and is accompanied by an additional release of water that is bound in the clay system of the host rocks, resulting in further increase in pore pressure.

In this workflow, we define forward modeling as obtaining vertical velocity models from pore pressures. First, effective stress is calculated for various pore pressure gradient scenarios by subtracting pore pressure from overburden stress. Second, effective stress is then converted into porosity using a compaction-diagenetic model. Finally, porosity is used to compute velocity via an attribute model, a velocity-porosity transformation. The forward modeling produces velocity rock physics templates (RPTs) corresponding to different pore pressure gradients. In the reverse direction, this workflow generates pore pressure predictions from an input of velocity.

SYNTHESIS OF 2D SEISMIC DATA

This section gives an overview of the seismic data. The data set we chose was acquired in the Gulf of Mexico at four millisecond sampling, using ocean bottom cables (OBC). The area where it was recorded has a shallow water depth, approximately 36 meters on average. We were provided with upgoing P-Z summed data. The source lines are perpendicular to the receiver lines. Source line spacing is 400 meters and source spacing is 50 meters, while receiver line spacing is 600 meters and receiver spacing is 50 meters. Maximum offset is about six kilometers.

To synthesize a 2D data set from the original 3D data, we chose a subset of the 3D data with midpoints within a one-kilometer swath, covering two receiver lines. Assuming structures do not vary significantly in the cross-line direction, the chosen sources and receivers were rotated about their midpoints to align in-line, sorted into 50-meter bins, and stacked to generate our 2D data. For more details on preprocessing, see Le et al. (2017b).

VELOCITY MODEL BUILDING

Figure 1 shows different pore pressure profiles (left panel), the RPTs (middle panel), and smectite fraction (right panel) modeled by our workflow at one of the wells. We observed that pore pressure is hydrostatic down to about 3 km deep where it starts to increase toward overburden pressure. This is also the depth where smectite-illite transformation begins. This deviation of pore pressure can be seen most prominantly in the figure's left panel, which shows mud weight data at this well.

Figure 2 shows mud weight data at four nearby wells (left panel) and different trial pressure profiles that we use to build velocity models for imaging (right panel). These different pressure profiles are transformed into the corresponding velocities and extrapolate along interpreted horizons. Figures 3a and 3b show the provided legacy velocity and the rock physics velocity. We have used the Top of Pliocene and Top of Miocene as guides for the extrapolation. In addition we have also built anisotropic model for η by inverting stacking η from anisotropic Normal Moveout. Figures 4a and 4b show two CMP gathers before and after anisotropic NMO. Figures 5a and 5b show the RMS and interval η. Because the data's offset range is limited to 6 km, we don't expect to recover reliable anisotropy beyond 2 km depth.

MIGRATION RESULTS

Figures 6 and 7 respectively show the migrated images using the legacy velocity model with and without anisotropy. The addition of an anisotropic η model improves the image's focusing by a small amount, and mostly in the shallow areas. Figures 8 and 9 respectively show the angle gathers of the two migrations. For a more quantitative accessment of these gathers, we have computed semblances by stacking along the

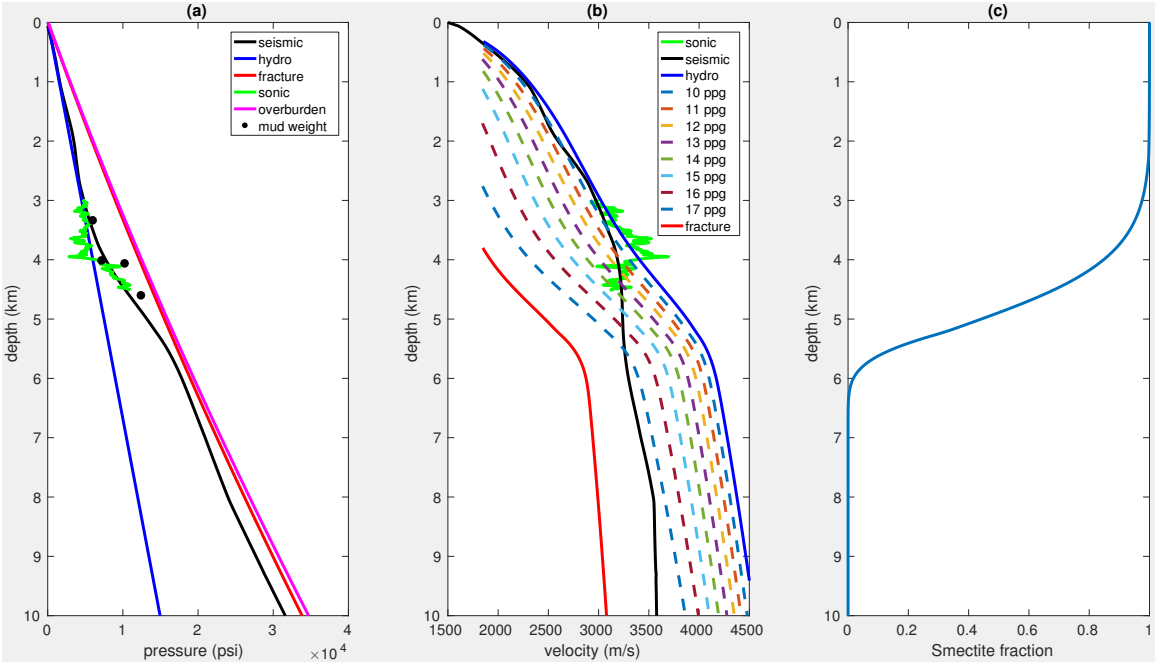

Figure 1: (a) Pore pressures, (b) RPTs, and (c) smectite fraction trends. [**CR**]

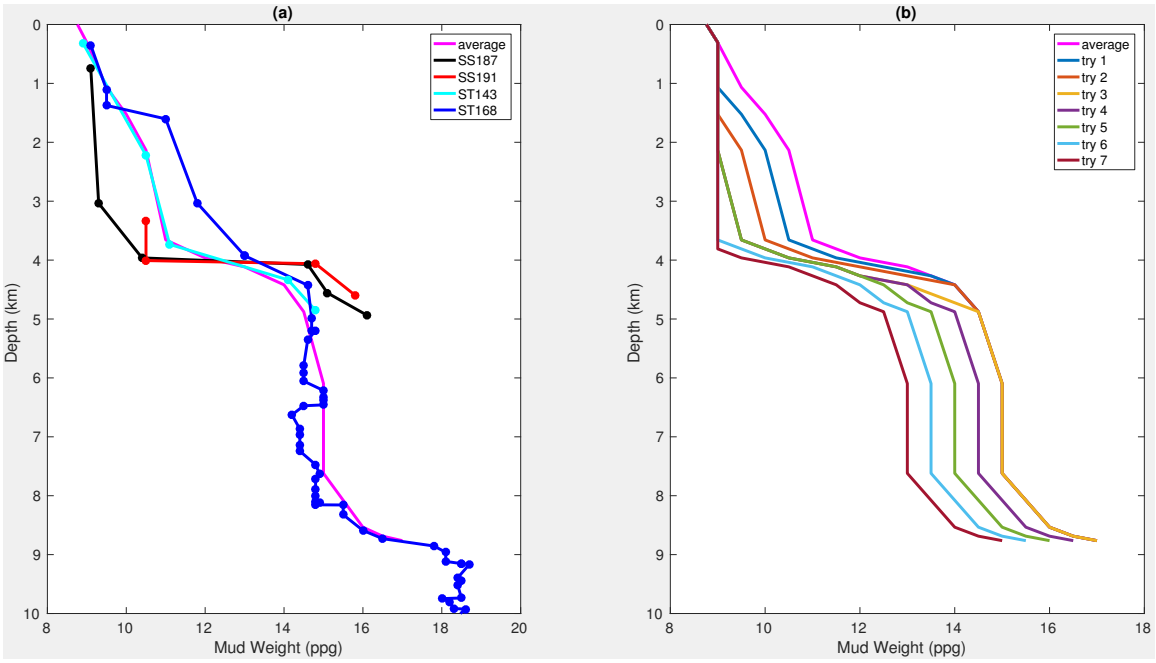

Figure 2: (a) Mud weight data at four nearby wells and (b) trials presssure profiles. [**CR**]

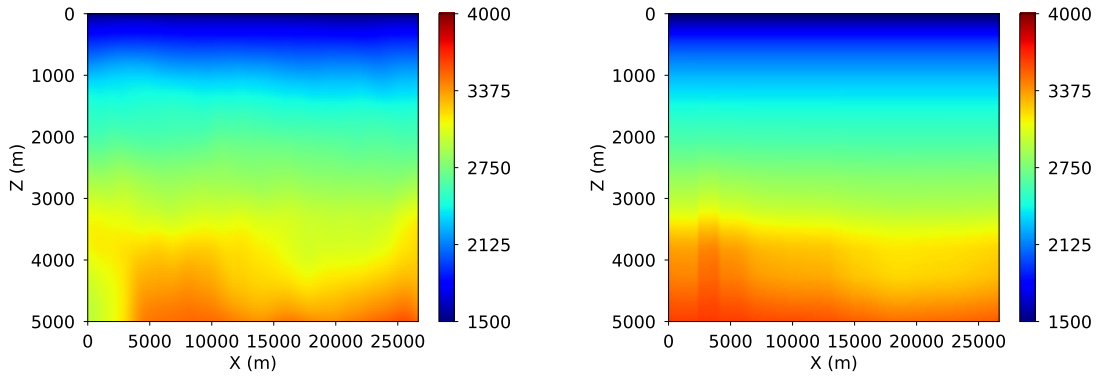

(a) (b)

Figure 3: (a) Legacy velocity model and (b) velocity model built from RPTs and average pressure profile. Notice a fault at about 2 km. [**CR**]

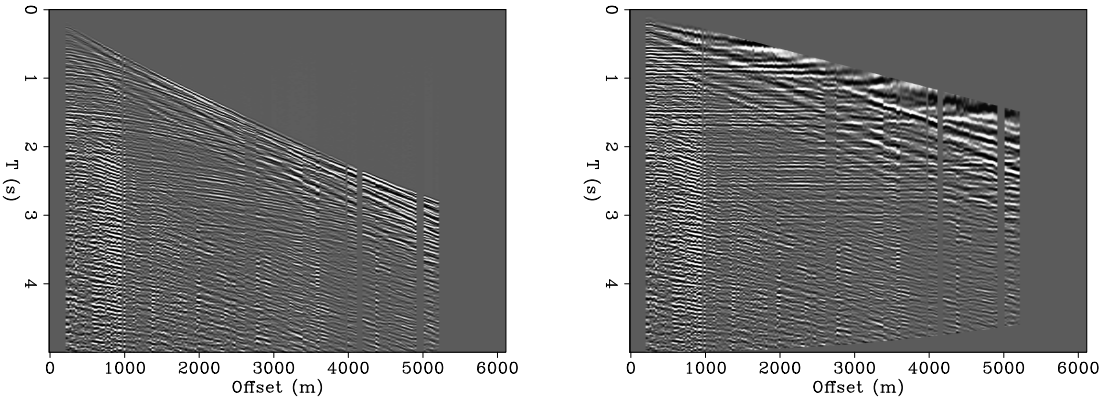

(a) (b)

Figure 4: CMP gather before (a) and after (b) anisotropic NMO. [**CR**]

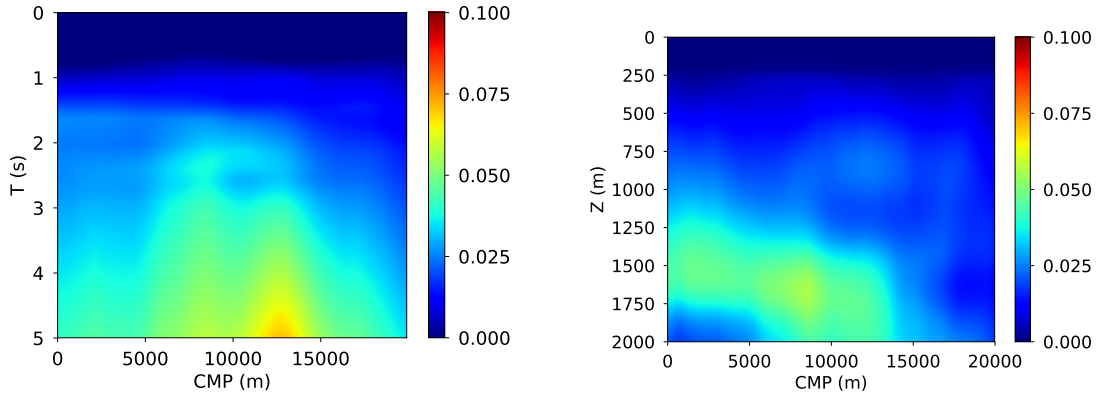

(a) (b)

Figure 5: (a) RMS and (b) interval η. [**CR**]

angle axis (Figures 10a and 10b). The semblance from stacking angle gather of the migrated image with anisotropy shows greater energy at the shallow part of the model, which can also be observed from the their histogram (Figure 10c).

Figures 11 and 12 respectively show the migrated images using the velocity model constructed with average pressure profile with and without anisotropy. In either migrations, the migrated images with constructed velocity display higher quality in terms of reflectors' focusing, particularly ones in the shallow regions of the model (2-4 km). Figures 13 and 14 show the corresponding angle gathers. The angle gathers obtained using pressure-converted velocity shows more flattened reflectors than those obtained with legacy velocity. Figures 15a and 15b show the semblances computed from these gathers. The semblance from angle gathers migrated with constructed velocity shows higher coherency, which is also illustrated by the histograms (Figure 16).

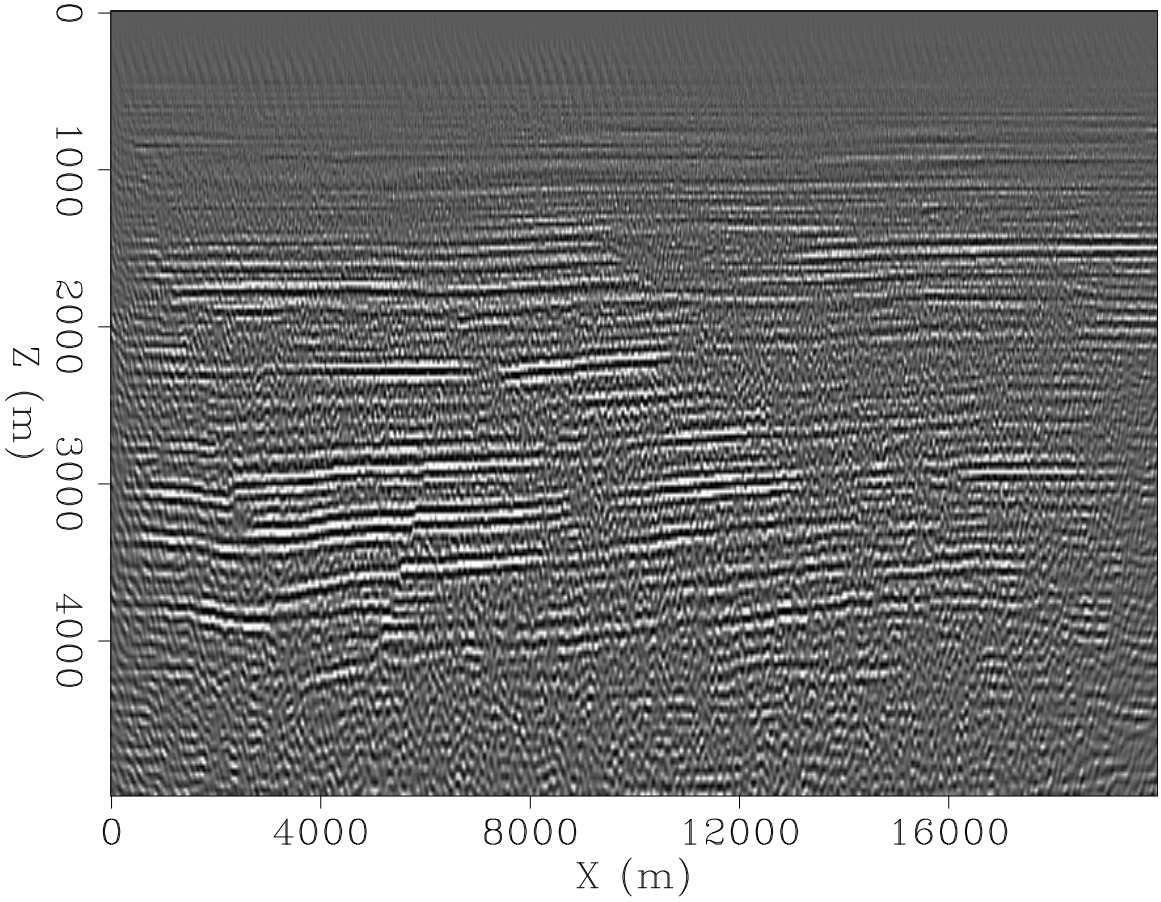

Figure 6: Migrated image with legacy velocity model. [**CR**]

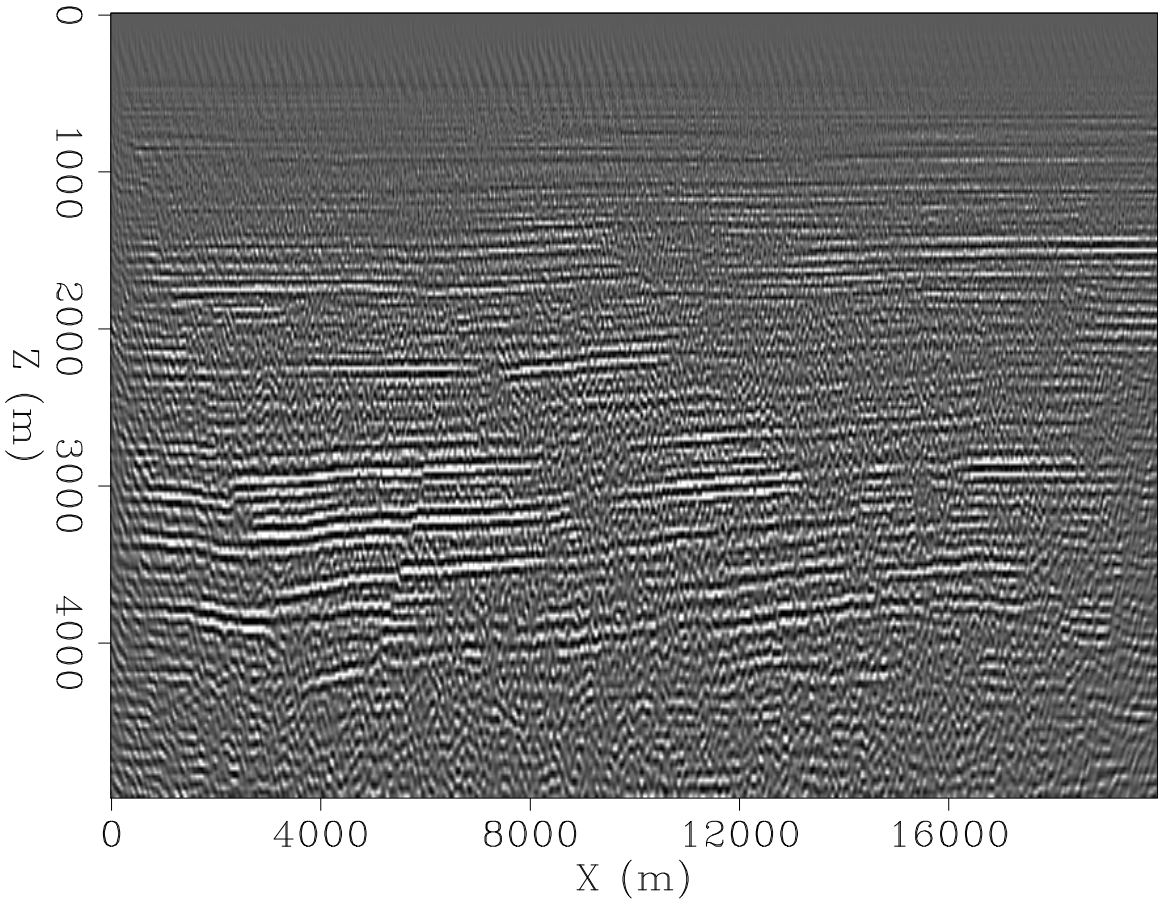

Figure 7: Migrated image with legacy velocity model and anisotropy. [**CR**]

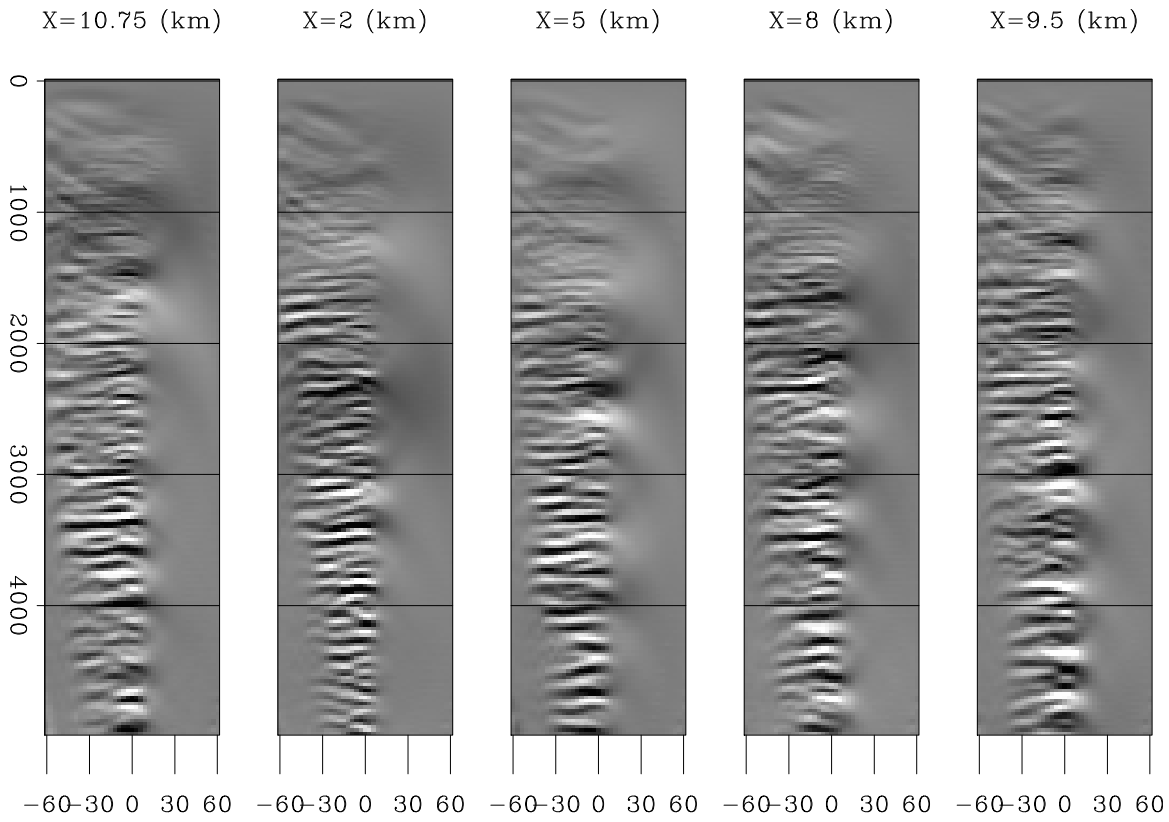

Figure 8: Angle gathers from isotropic migration with legacy velocity. [**CR**]

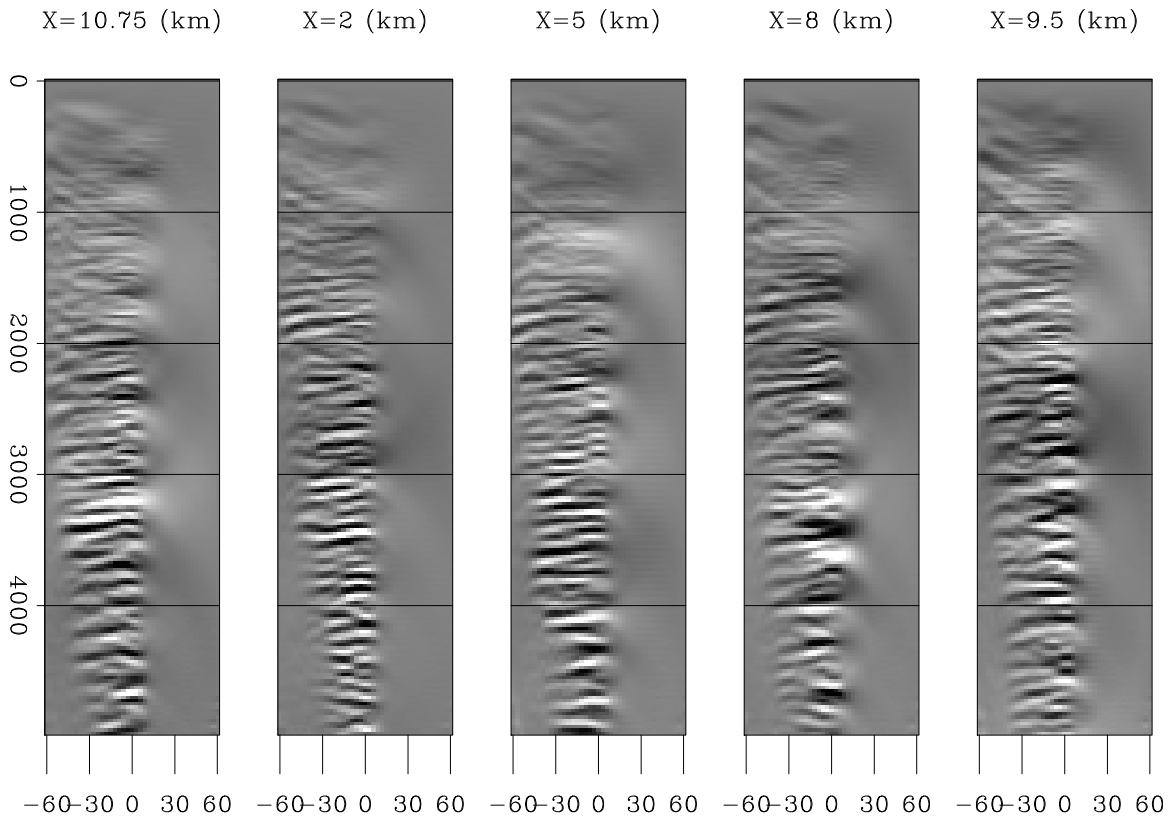

Figure 9: Angle gathers from anisotropic migration with legacy velocity and η. [**CR**]

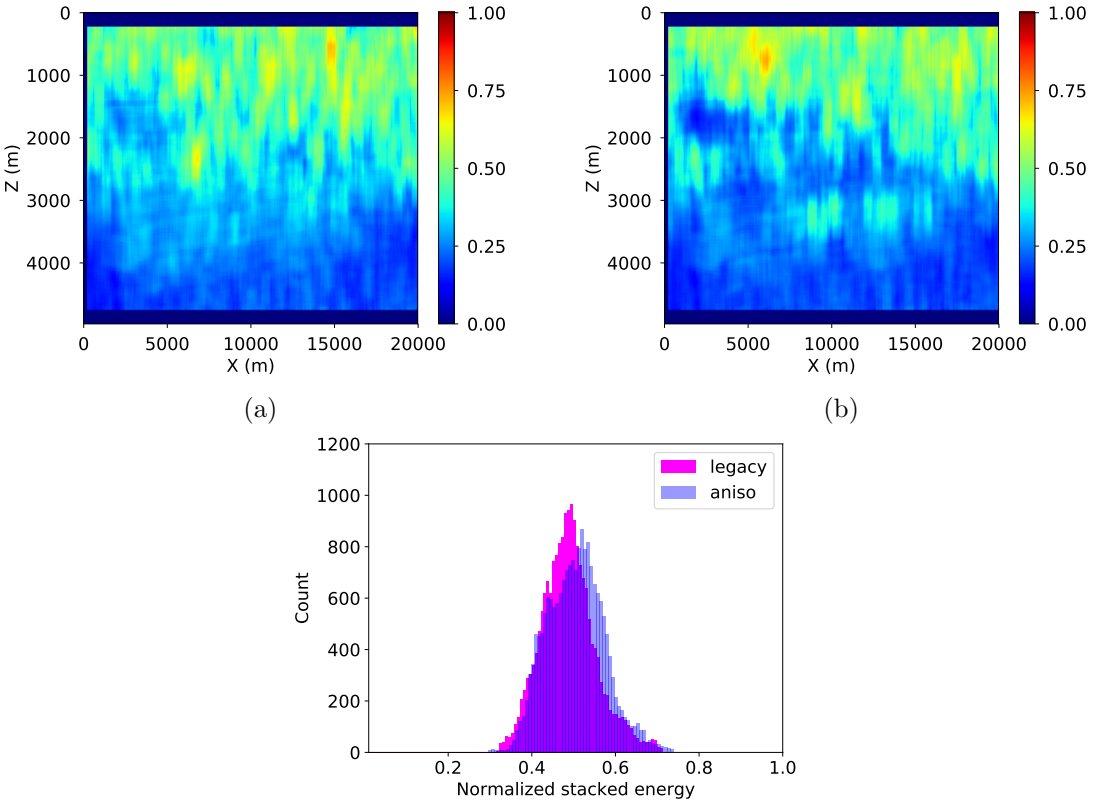

Figure 10: Semblances computed from angle gathers of isotropic (a) and anisotropic (b) migration with legacy velocity, and their corresponding hsitograms (c). [**CR**]

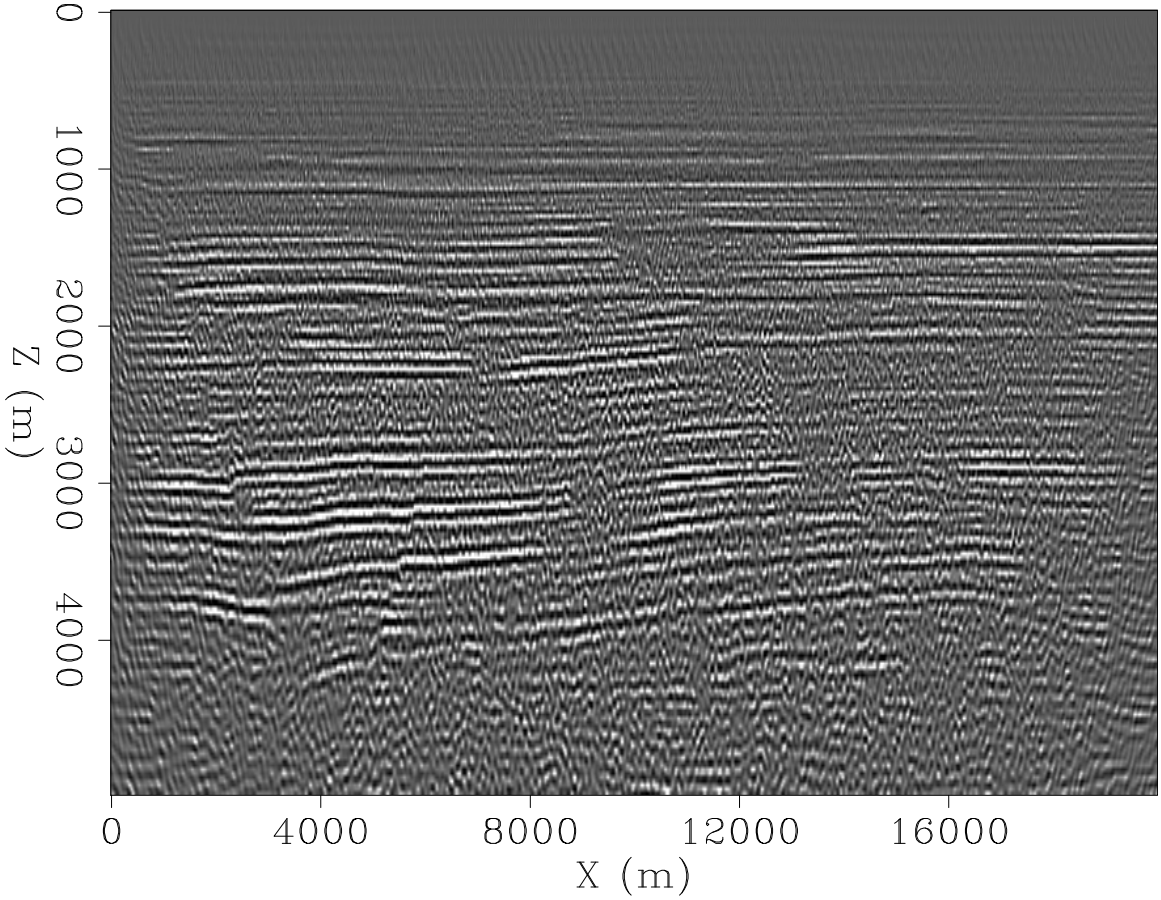

Figure 11: Migrated image with velocity constructed from average pressure profile. [**CR**]

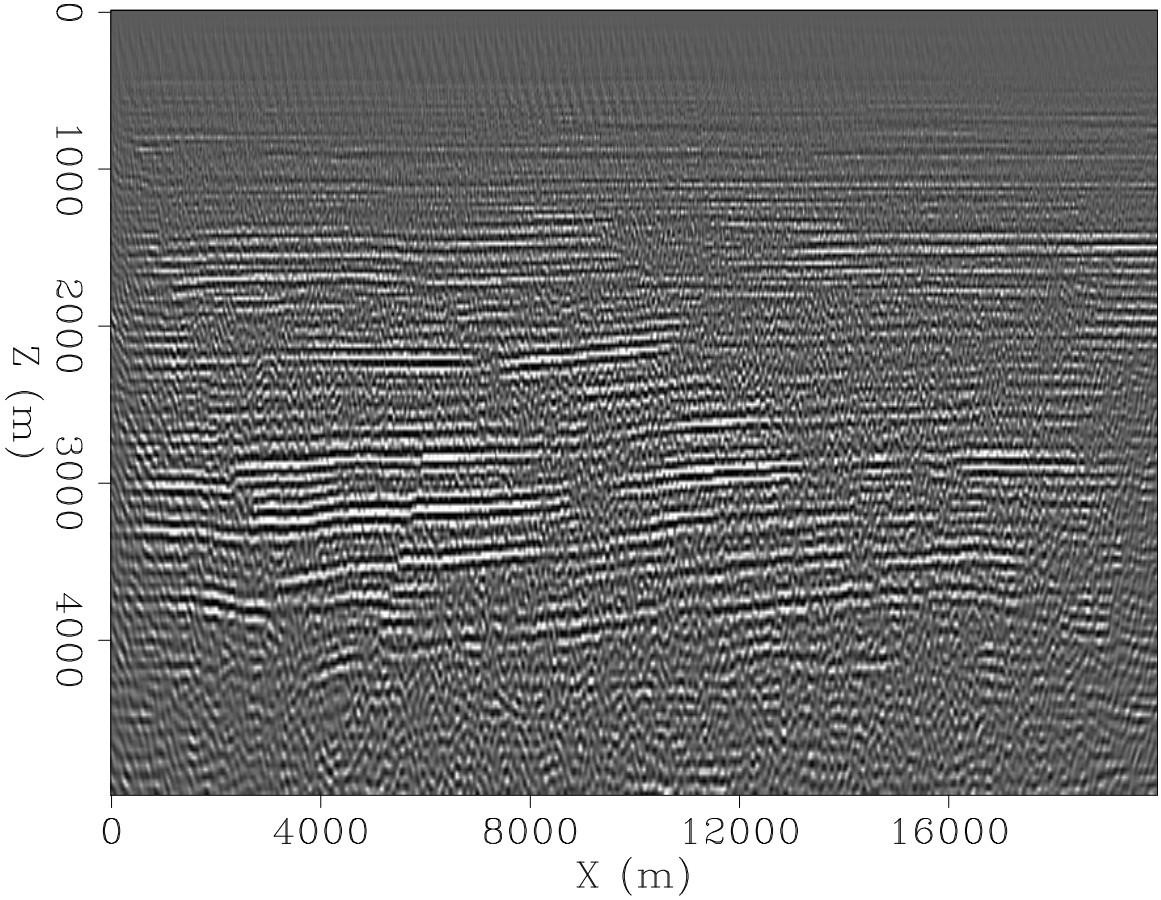

Figure 12: Migrated image with velocity constructed from average pressure profile and anisotropy. [**CR**]

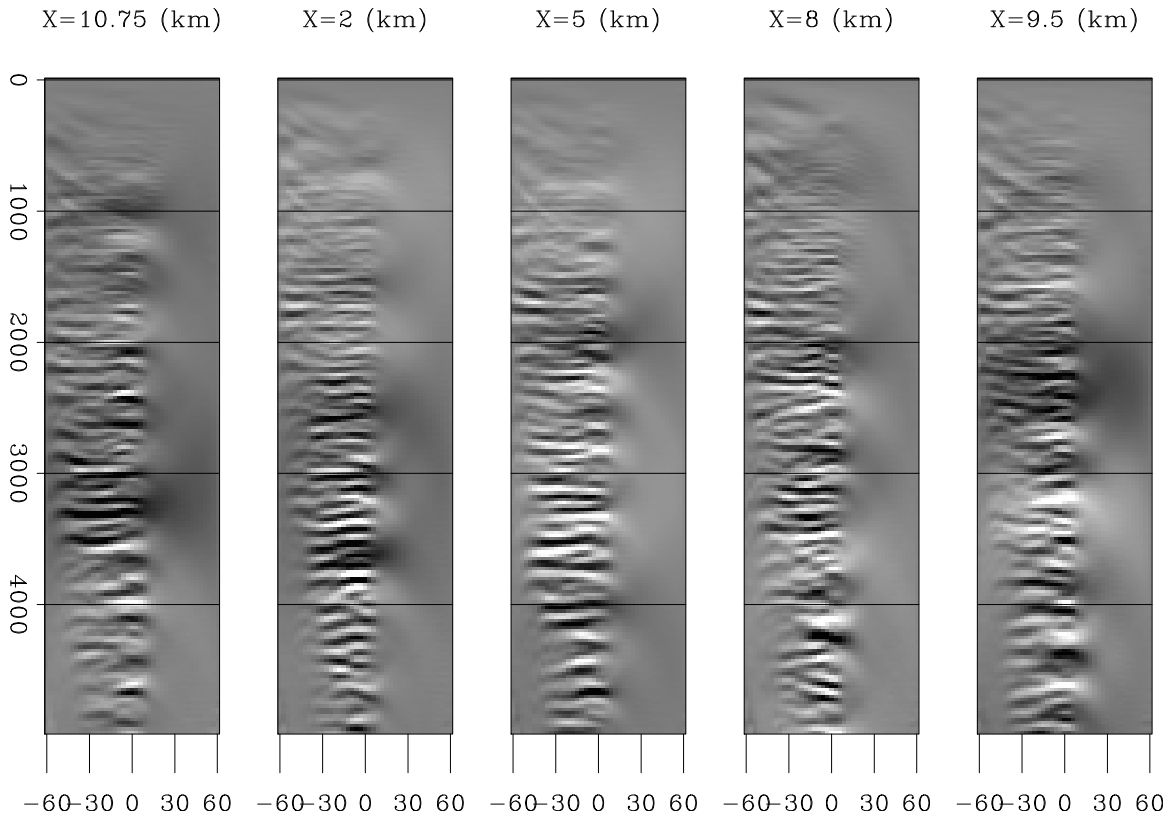

Figure 13: Angle gathers from isotropic migration with velocity constructed from rock physics and pore pressure constrained model (average pressure profile of Figure 2b. [**CR**]

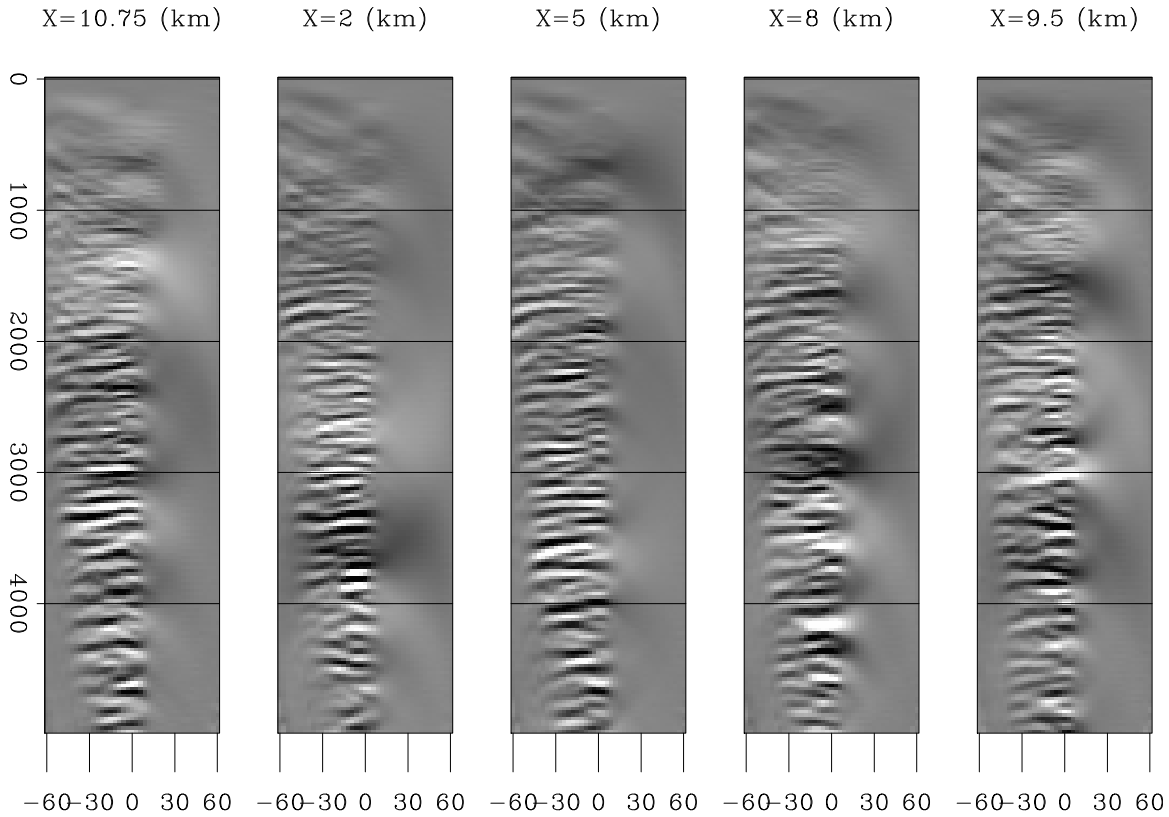

Figure 14: Angle gathers from anisotropic migration with velocity constructed from rock physics and pore pressure constrained model (average pressure profile of Figure 2b). [**CR**]

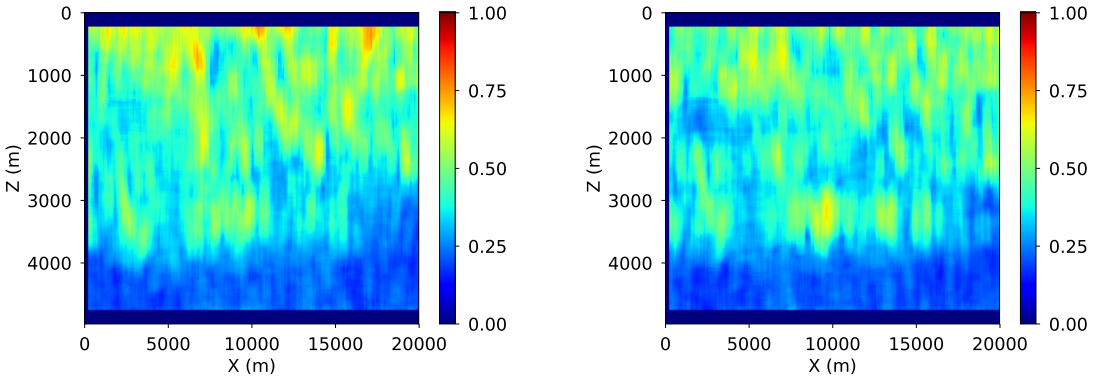

Figure 15: Semblances computed from angle gathers of isotropic (a) and anisotropic (b) migration with constructed velocity. [**CR**]

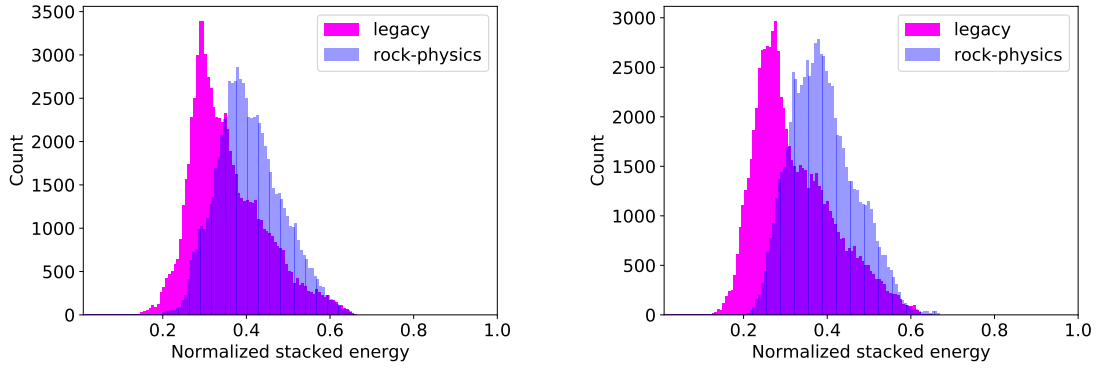

(a) (b)

Figure 16: Histograms of semblances from isotropic (a) and anisotropic migrations' angle gathers comparing between legacy velocity and constructed velocity. Histogram from the semblance of gathers migrated with constructed velocity shifts right compared to the one migrated with the legacy velocity, indicating higher coherency of angle gathers. [**CR**]

CONCLUSIONS

Following a rock physics guided workflow, we have built velocity templates and constructed a velocity model that seems to produce more focused migrated images and flattened angle gathers than those by the legacy model. Our velocity model reflects the deviation of pore pressure from hydrostatic where smectite-illite transformation occurs. Our ongoing work is to use this velocity model in a waveform inversion process with bound constraints from the velocity templates.

ACKNOWLEDGEMENTS

We would like to thank WesternGeco L.L.C. for providing us the seismic data and IHS Energy Log Services Inc. for the well logs. Thank Dr. Robert G. Clapp, Dr. Shuki Ronen, Dr. Allegra H. Scheirer, and Wisam H. AlKawai of the Geophysics and Geological Sciences Departments at Stanford University for insightful discussions. Thank the sponsors of the Stanford Exploration Project (SEP) and the Basin and Petroleum System Modeling Group (BPSM) for financial support.

REFERENCES

Bachrach, R., 2010, Applications of deterministic and stochasitc rock physics modeling to anisotropic velocity model building: SEG Annual International Meeting, Expanded Abstracts, 2436–2440, Society of Exploration Geophysicists.

Dutta, N., B. Deo, Y. K. Liu, Krishna, Ramani, J. Kapoor, and D. Vigh, 2015, Pore-

pressure-constrained, rock-physics-guided velocity model building method: Alternate solution to mitigate subsalt geohazard: Interpretation, **3**, SE1–SE11.

Dutta, N. C., 2002, Geopressure prediction using seismic data: Current status and the road ahead: Geophysics, **67**, 2012–2041.

Le, H., S. A. Levin, and R. G. Clapp, 2017a, Synthesis, processing, and migration of a 2D data from the Gulf of Mexico : SEP-Report, **170**, 17–24.

Le, H., A. Pradhan, N. Dutta, B. Biondi, T. Mukerji, and S. A. Levin, 2017b, Building pore pressure and rock physics guides to constrain anisotropic waveform inversion : SEP-Report, **170**, 1–12.

Li, Y., B. Biondi, R. Clapp, and D. Nichols, 2016, Integrated VTI model building with seismic data, geological information, and rock-physics modeling-Part 1: Theory and synthetic test: Geophysics, **81**, C177–C191.

Matava, T., R. Keys, D. Foster, and D. Ashabranner, 2016, Isotropic and anisotropic velocity-model building for subsalt seismic imaging: The Leading Edge, **35**, 240–245.

Petmecky, R. S., M. L. Albertin, and N. Burke, 2009, Improving sub-salt imaging using 3d basin model derived velocities: Marine and Petroleum Geology, **26**, 457–463.